INORGANIC CHEMISTRY
FRONTIERS

RESEARCH ARTICLE

View Article Online
View Journal | View Issue

Cite this: *Inorg. Chem. Front.*, 2025, **12**, 2856

Determining the zero-field cooling/field cooling blocking temperature from AC susceptibility data for single-molecule magnets†‡

Yolimar Gil, [a] María Mar Quesada-Moreno, *[b] María A. Palacios, [c] Silvia Gómez-Coca,*[d] Enrique Colacio, *[c] Eliseo Ruiz *[d] and Daniel Aravena *[e]

Received 18th December 2024,
Accepted 11th February 2025

DOI: 10.1039/d4qi03259d

rsc.li/frontiers-inorganic

We present a general relationship between the magnetisation blocking temperature (T_B) measured using the zero-field cooling/field cooling technique (ZFC/FC) and the temperature-dependent spin relaxation time obtained from AC susceptibility and magnetisation decay measurements. The presented mathematical approach supplies ZFC/FC blocking temperatures at any heating rate (R_H), providing comparable values to those obtained experimentally, as demonstrated by testing 107 examples for reported single-molecule magnets (SMMs) where the ZFC/FC curve has been measured. This procedure is examined in further detail for a new single-molecule magnet, $[Dy(OPAd_2Bz)_2(H_2O)_4Br]Br_2{\cdot}4THF$ (**1**) ($OPAd_2Bz$: di(1-adamantyl)benzylphosphine oxide). For this compound, ZFC/FC measurements were made over a broad range of heating rates (0.01–5 K min^{-1}), which agreed with the general behaviour predicted from AC susceptibility data. We discuss how the demagnetisation mechanism determines the sensitivity of T_B with respect to the heating rate: T_B is mostly insensitive to R_H for Orbach relaxation, while there is a larger sensitivity for Raman-limited systems. Our conclusions provide a clear physical interpretation of ZFC/FC blocking temperatures, aiding in the proper contextualization of this figure of merit.

Introduction

In the early 1990s, the discovery of single molecule magnets (SMMs) sparked a revolution in the field of molecular magnetism. These molecular transition metal coordination compounds exhibit a magnetic memory effect, which arises from blocking magnetisation *via* an anisotropic barrier (U_{eff}) for prolonged periods in the absence of an external magnetic field and below a critical temperature known as the blocking temperature (T_B).[1–5] SMMs have been extensively investigated due to their immense technological potential in molecular spintronics, ultra-high-density data storage, and quantum information technologies using spin qubits.[6–12]

However, a significant challenge in the field remains, necessitating the achievement of a magnetic memory effect at practical/high temperatures while maintaining high thermal stability in the presence of air and humidity.[13,14] Mononuclear SMM complexes exhibit modulable magnetic anisotropy through chemical tuning of their coordination environment, representing the smallest nanomagnets which can be modulated by the rational selection of metal ions and ligands.[15–26] Notably, the Dy^{III} ion, with its unquenched orbital momentum and large magnetic anisotropy, has emerged as a leading candidate to revolutionize technology based on electron spin.[15–20,27–29]

Experimental and computational studies have revealed that strong axial crystal fields, achieved through axial distribution of ligands, are crucial for Dy^{III} complexes to exhibit remarkable SMM behaviour.[15–20,30–32] More recent approaches seek to attenuate vibrational displacements to hamper Raman relaxation.[33,34] For future systems, some theoretical works suggest exploring the surface deposition of SMMs and uncommon oxidation states.[35,36] In the quest to develop practical SMM applications, reaching a blocking temperature (T_B) above

[a]*Facultad de Ciencias Químicas y Farmacéuticas, Universidad de Chile, Casilla 233, Santiago, Chile*
[b]*Departamento de Química Física y Analítica, Universidad de Jaén, Campus Las Lagunillas, 23071 Jaén, Spain. E-mail: mqmoreno@ujaen.es*
[c]*Departamento de Química Inorgánica, Facultad de Ciencias, Universidad de Granada, 18071Granada, Spain. E-mail: ecolacio@ugr.es*
[d]*Departament de Química Inorgànica i Orgànica and Institut de Recerca de Química Teòrica i Computacional, Universitat de Barcelona, Diagonal 645, 08028 Barcelona, Spain. E-mail: silvia.gomez.coca@ub.edu, eliseo.ruiz@qi.ub.edu*
[e]*Departamento de Química de los Materiales, Facultad de Química y Biología, Universidad de Santiago de Chile, Casilla 40, Correo 33, Santiago, Chile. E-mail: daniel.aravena.p@usach.cl*

†We want to dedicate this paper to Prof. Miquel Julve from the Universitat de Valencia, who recently passed away.

‡Electronic supplementary information (ESI) is available. CCDC 2372498. For ESI and crystallographic data in CIF or other electronic formats, see DOI: https://doi.org/10.1039/d4qi03259d.

liquid nitrogen temperature (77 K) is crucial. There are only two molecules that have surpassed this crucial barrier; both of them are Dy compounds. Mononuclear Dy^{III} [$Dy(C_5Me_5(Cp^{iPr5}))][B(C_6F_5)_4]$][37] and mixed-valence $Dy^{III}Dy^{II}$ dinuclear [$Dy_2I_3(Cp^{iPr5})_2$] metallocene[38] compounds have achieved landmark performances with U_{eff} = 2217 K and 2347 K, respectively, and T_B = 80 K in both cases. The uniaxial local symmetry stabilizes the largest m_J = ±15/2 ground state[39,40] in the former, and the collinearity of the local anisotropic axes and the strong 4f-radical coupling in the latter, results in a significant separation from the first and higher excited states.[38,41,42] However, compounds with such low coordination are unstable and the need for more stable systems with similar magnetic properties arises. Different high-order symmetry axes, such as those found in trigonal bipyramidal (D_{3h}),[43,44] square antiprismatic (D_{4d}),[45–49] sandwich,[37,50–54] and pentagonal bipyramidal (D_{5h}),[55–73] have been recommended to favour slower relaxation of magnetisation by reducing transverse anisotropy and suppressing quantum tunnelling of the magnetisation (QTM). The presence of a high-order symmetry axis also promotes the collinearity of anisotropic axes of the excited and ground states, leading to larger U_{eff} values.[74,75] Nonetheless, it is essential to engineer molecular vibrations to control the spin lifetime of SMM complexes,[76] as flexible lattices are responsible for fast relaxation. Addressing the requirements of high-temperature performance and thermal air and humidity stability, mononuclear Dy^{III} SMMs with D_{5h} geometry hold a fair position, displaying, in many cases, stability against these factors with U_{eff} and T_B values as high as 1162 K [63] and 36 K,[70] respectively. Although some recent mononuclear Dy^{III} SMMs with D_{5h} geometry have been shown to be air-sensitive, the majority are stable.[60,61,73,77] Recently, the role of spin-vibrational coupling in designing high-performance pentagonal bipyramidal Dy^{III} SMMs was revealed using a combination of density functional theory (DFT) and complete active space self-consistent field (CASSCF) calculations.[33] There are about thirty examples of mononuclear Dy^{III} SMMs with D_{5h} geometry, but those employing axial bulky phosphine oxide type ligands (high electron density) and weak donor equatorial ones (*e.g.*, water)[56–59,62,64] are relatively scarce. These D_{5h} based SMMs represent a highly efficient approach for constructing new high-performance SMMs.

As mentioned previously, the Dy^{III} metallocene compounds [$Dy(C_5Me_5(Cp^{iPr5}))][B(C_6F_5)_4]$] and [$Dy_2I_3(Cp^{iPr5})_2$] show the highest blocking temperature reported to date. This value was measured as the maximum temperature at which magnetic hysteresis is observed (herein T_{B-H}). However, there are two other ways to quantify the blocking temperature: the temperature at which the magnetic relaxation time is equal to 100 s ($T_{B\text{-}100}$) and the maximum of the zero-field cooled (ZFC) magnetic susceptibility ($T_{B\text{-}ZFC/FC}$). For the dysprosium metallocene cation, these values are 67 and 52 K, respectively. This example indicates how different the blocking temperature can be depending on the measurement technique. Furthermore, key experimental parameters can also influence T_B significantly. In the case of magnetic hysteresis measurements, T_{B-H} varies with the field sweep rate, where faster sweep rate programs lead to higher blocking temperatures. Focusing on ZFC/FC experiments, $T_{B\text{-}ZFC/FC}$ is sensitive to the heating rate, with faster heating rates leading to higher blocking temperatures. Unfortunately, the experimentally employed heating rate is often missing from reports in the literature, hindering a rigorous comparison between systems from different publications. Another issue is related to a misunderstanding of the definition of $T_{B\text{-}ZFC/FC}$, since some authors refer to this value as the temperature where the ZFC and FC curves diverge, which corresponds to the irreversibility temperature (T_{irrev}) and is higher than that of $T_{B\text{-}ZFC/FC}$.[78] Although $T_{B\text{-}100}$ usually does not depend strongly on the measurement conditions, the 100 s definition is arbitrary and it is not clear why the blocking temperature at this specific relaxation time is more informative of SMM behaviour than other thresholds. Blocking temperatures are convenient as "single-molecule magnet" performance metrics since they condense a complex magnetic relaxation dependence into a single figure. Moreover, the existence of a magnetic blocking temperature provides a clear definition of a "molecular magnet" that goes beyond the presence of slow relaxation of magnetisation. However, other demagnetisation parameters, such as magnetic coercivities or demagnetisation barriers (U_{eff}) are also relevant for the assessment of SMM performance.

In this paper, we propose a new approach for estimating $T_{B\text{-}ZFC/FC}$ at any heating rate from the temperature-dependent spin relaxation time obtained from AC susceptibility and magnetisation decay measurements, to advance towards a more harmonized definition of T_B. In this way, $T_{B\text{-}ZFC/FC}$ data from different studies can be better compared, as many examples of ZFC/FC experiments in the literature do not state the heating rate. Furthermore, the model allows for the estimation of $T_{B\text{-}ZFC/FC}$ in cases where the ZFC/FC experiment was not done. Experimentally, performing the ZFC/FC experiment together with AC magnetometry measurements is not a practical problem, so the main use of our proposed method is not to avoid the ZFC/FC experiment but to provide a new tool to contextualize and estimate ZFC/FC blocking temperatures.

To validate this new model, we compared $T_{B\text{-}ZFC/FC}$ values for 107 examples of SMMs from the literature for which ZFC/FC data were reported, including both lanthanide and transition metal systems. Furthermore, we conducted a detailed AC susceptibility and ZFC/FC study for a new Dy^{III} SMM with D_{5h} geometry. Concretely, we measured ZFC/FC curves for a wide range of heating rates, demonstrating that the presented model accurately predicted $T_{B\text{-}ZFC}$ values and captured the heating rate dependence of the blocking temperature.

Results and discussion

Mathematical model for ZFC/FC blocking temperature determined from AC susceptibility

Our first goal is relating the blocking temperature measured by zero field cooling experiments with an expression in terms

of the temperature dependent relaxation time. Experimentally, susceptibility is calculated as the ratio between the magnetic moment and the applied magnetic field. The isothermal (static) susceptibility is:

$$\chi_T = \frac{M_{eq}}{B} = \frac{gS(P_\uparrow - P_\downarrow)_{eq}}{B} \quad (1)$$

where M_{eq} is the magnetic moment corresponding to the equilibrium population at a given temperature and magnetic field (B), g is the Landé factor, S is the spin and $P_\uparrow - P_\downarrow$ is the population difference between spin up and down species. The expression for non-equilibrium susceptibility measured in the ZFC experiment is analogous to eqn (1) when the magnetic moment $P_\uparrow - P_\downarrow$ term is out of equilibrium.

Combining the equilibrium and out of equilibrium expressions for magnetic susceptibility, χ_{ZFC} is defined as:

$$\begin{aligned}\chi_{ZFC} &= \frac{(P_\uparrow - P_\downarrow)}{(P_\uparrow - P_\downarrow)_{eq}}\chi_T \\ &= \chi_T\left[\frac{(P_\uparrow - P_\downarrow) - (P_\uparrow - P_\downarrow)_{eq}}{(P_\uparrow - P_\downarrow)_{eq}} + 1\right] \\ &= \chi_T\left[\frac{\Delta M}{(P_\uparrow - P_\downarrow)_{eq}} + 1\right]\end{aligned} \quad (2)$$

The numerator on the r.h.s. of eqn (2) is the difference between the equilibrium and out of equilibrium magnetic moments (ΔM).

The kinetic equation for a system after a perturbation is:

$$\frac{d\Delta M}{dt} = -\tau^{-1}(T)\Delta M \quad (3)$$

where the relaxation rate τ^{-1} is temperature dependent. In the ZFC experiment, the sample is initially cooled in the absence of an external direct magnetic field. After reaching a cryogenic temperature, the magnetic moment is measured using a small magnetic field and the sample is heated at a rate of R_H (K s^{-1}): Hence, eqn (3) becomes:

$$\frac{d\Delta M}{dT} = -\tau^{-1}(T)\Delta M/R_H \quad (4)$$

The general solution of eqn (4) is:

$$\Delta M = C_1 \exp\left(-{R_H}^{-1}\int \tau^{-1} dT\right) \quad (5)$$

where C_1 is the magnetisation at the beginning of the ZFC heating step; if all spins remain frozen when the magnetic field needed for the measurement of the heating curve is turned on, $C_1 = -\tanh\left(-\frac{\beta gSB}{T}\right)$ and the combination of eqn (2) and (5) yields the simple form:

$$\chi_{ZFC} = \chi_T\left[-\exp\left(-{R_H}^{-1}\int \tau^{-1} dT\right) + 1\right] \quad (6)$$

In practice, the magnetic moment is not zero at the beginning of the heating step. This is the typical situation in ZFC/FC experiments and depends on the orientational distribution of magnetic moments, their alignment with respect to the external field and operational parameters, as the time needed to stabilize the initial temperature in each experiment. Since this parameter is sample and experiment dependent, we assume it is an effective constant, C_1', with a value between 0 and 1. In this way, eqn (7) becomes:

$$\chi_{ZFC} = \chi_T\left[-C_1' \exp\left(-{R_H}^{-1}\int \tau^{-1} dT\right) + 1\right] = \lambda\chi_T \quad (7)$$

where the term in parentheses is the fraction of relaxed magnetic moments ($0 \le \lambda \le 1$). Eqn (7) allows for the determination of the blocking temperature by the evaluation of the maximum of χ_{ZFC} for an arbitrary χ_T. Importantly, eqn (7) can be applied to different experimental conditions (such as the presence of magnetic fields) if these effects are present in the data that produced the τ^{-1} function. Although all results from this paper can be obtained from eqn (7), we are also interested in an analytical expression for T_B. Thus, the maximum of χ_{ZFC} is expressed as:

$$\begin{aligned}\frac{d\chi_{ZFC}}{dT}(T_B) &= 0 \\ &= \frac{d\chi_T}{dT} - \frac{d\chi_T}{dT}C_1' \exp\left(-{R_H}^{-1}\int_0^{T_B} \tau^{-1} dT\right) \\ &\quad + \chi_T {R_H}^{-1}\tau^{-1}(T_B)C_1' \exp\left(-{R_H}^{-1}\int_0^{T_B} \tau^{-1} dt\right)\end{aligned} \quad (8)$$

$$\begin{aligned}&\chi_T {R_H}^{-1}\tau^{-1}(T_B)C_1' \exp\left(-{R_H}^{-1}\int_0^{T_B} \tau^{-1} dT\right) \\ &= \frac{d\chi_T}{dt}\left[-1 + C_1' \exp\left(-{R_H}^{-1}\int_0^{T_B} \tau^{-1} dT\right)\right]\end{aligned} \quad (9)$$

$$\chi_T / \frac{d\chi_T}{dt} = \frac{R_H\left[-1 + C_1' \exp\left(-{R_H}^{-1}\int_0^{T_B} \tau^{-1} dT\right)\right]}{\left[\tau^{-1}(T_B)C_1' \exp\left(-{R_H}^{-1}\int_0^{T_B} \tau^{-1} dT\right)\right]} \quad (10)$$

For simplicity, we consider that the isothermal susceptibility reasonably follows the Curie law:

$$\chi_T / \frac{d\chi_T}{dt} = -T_B \quad (11)$$

The assumption of the Curie law greatly simplifies the following equations but can be reversed if needed.

Hence, the blocking temperature is:

$$T_B = \frac{R_H\left[1 - C_1' \exp\left(-{R_H}^{-1}\int_0^{T_B} \tau^{-1} dT\right)\right]}{C_1' \exp\left(-{R_H}^{-1}\int_0^{T_B} \tau^{-1} dT\right)\tau^{-1}(T_B)} \quad (12)$$

Eqn (12) can be expressed in a way that the l.h.s. coincides with the term in square brackets from eqn (7):

$$1 - C_1' \exp\left(-{R_H}^{-1}\int_0^{T_B} \tau^{-1} dT\right) = \frac{T_B}{T_B + R_H\tau(T_B)} \quad (13)$$

Thus, the blocking temperature can be estimated by knowing the heating rate, the temperature dependence of τ

and C_1'. In summary, T_B can be obtained from either eqn (7) or (12), where the latter expression gives an explicit term for T_B by assuming the Curie law. We analysed how these two approaches performed for a selected group of experimental examples from the literature (see section 4 and Table S8 in the ESI‡) and concluded that both equations provided satisfactory results for T_B, especially for larger values of C_1'. In general, the Curie law assumption from eqn (13) gives slightly lower calculated T_B values than eqn (7), which employs the experimental dependence of χ. In conclusion, we recommend employing either of the equations with $C_1' = 1$ to obtain reliable estimations for $T_{B\text{-ZFC/FC}}$.

Synthesis and characterization of the Dy^{III} SMM with D_{5h} geometry

In view of previous considerations, we focused our efforts on the preparation of a mononuclear Dy^{III} coordination complex, $[Dy(OPAd_2Bz)_2(H_2O)_4Br]Br_2{\cdot}4THF$ (**1**) ($OPAd_2Bz$: di(1-adamantyl)benzylphosphine oxide), close to ideal pentagonal bipyramidal geometry, which fulfilled all the desired characteristics to obtain SMMs with high U_{eff} and T_B values, that is, a strong axial crystal field, humidity and air stability, and a rigid network to avoid rapid relaxation. A strong axial crystal field is created by the two bulky di(1-adamantyl)benzylphosphine oxide ligands located in the axial positions, which lead to a magnetic hysteresis that remains open up to 14 K, one of highest values for air/humidity stable SMMs synthesized to date. Four water molecules and one bromide anion are located in the equatorial positions; this is structurally different from previous compounds with axial phosphine oxide ligands, where five water molecules are located instead.[56–59,62] Furthermore, we provide detailed insights into the mechanism that governs the magnetic relaxation of complex **1** by using *ab initio* CASSCF based computational methods.

Complex **1** was prepared by the solvothermal reaction of the di(1-adamantyl)benzylphosphine oxide ligand with anhydrous $DyBr_3$ in anhydrous tetrahydrofuran and in a 2 : 1 molar ratio using a 23 mL Teflon-lined stainless steel container and keeping it at 100 °C for three days (see ESI‡ for further details). The resulting solution from the solvothermal reaction was allowed to evaporate at room temperature for several days, whereupon large colourless prismatic single-crystals of $[Dy(OPAd_2Bz)_2(H_2O)_4Br]Br_2{\cdot}4THF$ (**1**) were obtained, which were air-stable (Fig. 1).

The molecular structure of **1** consists of $[Dy(OPAd_2Bz)_2(H_2O)_4Br]^{2+}$ cationic units, with are charge balanced by two free bromide anions, and four crystallization THF molecules (Figs. 1 and S3‡). The bromide anions and THF molecules interact with the cationic unit *via* hydrogen bonds. Within the cationic unit, the seven-coordinate Dy^{III} centre exhibits a pentagonal bipyramidal geometry (PBPY-7), very close to an ideal D_{5h} polyhedron, as supported by the continuous shape measurement analysis,[79] which provides an S(PBPY-7) value of 0.948 (where 0 corresponds to the ideal D_{5h} geometry) (Table S1, ESI‡). Two bulky $OPAd_2Bz$ ligands occupy the axial positions, whereas four water molecules and one bromide ion are in the equatorial plane (Fig. 1). The axial Dy–O1 distances

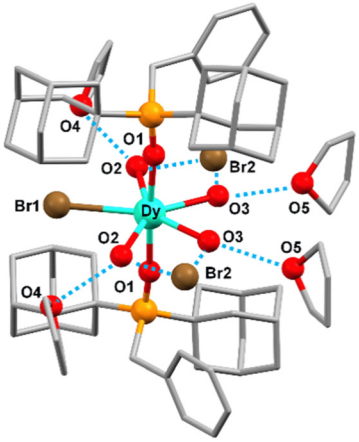

Fig. 1 Perspective view of the molecular structure of $[Dy(OPAd_2Bz)_2(H_2O)_4Br]Br_2{\cdot}4THF$ (**1**). Code colours: dysprosium (cyan), oxygen (red), bromide (brown), phosphorus (orange), and carbon (grey). Hydrogen atoms are omitted for clarity. Blue dashed lines indicate hydrogen bond interactions.

(2.210(3) Å) are shorter than the equatorial Dy–O2/O3 (average value of 2.365 Å) and Dy–Br1 (2.8860(6) Å) ones; this indicates that the cationic unit shows a compressed PBPY-7 geometry with an almost linear axial O1–Dy–O1 angle (176.73(16)°) and equatorial Br1–Dy–O2, O2–Dy–O3 and O3–Dy–O3 angles of 74.24(9)°, 71.88(13)° and 68.12(17)°, respectively, close to the ideal angle of 72° (Table S3, ESI‡). The coordinated bromide atom seems to generate certain steric repulsion with the water molecules close to it, which is reflected in a Br1–Dy–O2 angle greater than 72°. In turn, this brings about the closeness between these two water molecules and the other two, thus showing O2–Dy–O3 and O3–Dy–O3 angles less than 72°. The P–O1–Dy angle is also very close to linearity (173.67(19)°) and the angles between the equatorial and axial atoms are around 90° (Table S3, ESI‡). Specifically, the local symmetry of the DyO_6Br coordination sphere is C_{2v}, with the C_2 axis lying along the line connecting the coordinated bromide anion and the Dy^{III} ion (Fig. 1). Each coordinated water molecule interacts with one free bromide anion and one THF molecule *via* hydrogen bonds. The O2···Br2 and O3···Br2 donor–acceptor distances show respective values of 3.161(4) Å and 3.154(3) Å, whereas those for the O2···O4(THF) and O3···O5(THF) donor–acceptor distances are 2.802(6) Å and 2.774(19) Å, respectively. Moreover, the shortest Dy···Dy intermolecular distance for **1** is 12.1090(3) Å, which indicates that the $[Dy(OPAd_2Bz)_2(H_2O)_4Br]^{2+}$ units are well separated in the structure. There are no π···π stacking interactions between the aromatic benzene rings of different units. The free bromide atoms establish van der Waals interactions with the benzene hydrogens inside the same unit (3.0386(5) Å), and with the hydrogens of the CH_2 (2.6475(5) Å) and adamantyl groups (2.7673(5) Å) of adjacent units (Fig. S3‡).

Magnetic measurements

The DC magnetic properties of **1** were studied over the 2–300 K temperature range under an applied magnetic field of 0.5 T

and magnetisation was studied over the field range of 0–7 T at temperatures between 2 and 7 K, see Fig. S4.‡ It is worth noting that the obtained curves clearly show the typical features of magnetisation blocking in an efficient mononuclear Dy^{III}-SMM (sharp decrease of $\chi_M T$ at low temperature, sinusoidal behaviour of magnetisation at low field, divergence between FC and ZFC magnetic susceptibilities at low temperature, and magnetic hysteresis; see below and the magnetic studies section in the ESI‡).

The ZFC/FC magnetic susceptibilities were collected at two magnetic fields and over a wide range of heating rates to evaluate T_B and compare it with the proposed model (see Fig. 2). For the small field, 50 Oe, at very low heating rates, the ZFC/FC curves separate slightly at very low temperatures (Fig. S5‡). When increasing the heating rate, the ZFC and FC curves differ more and the temperatures at which the curves diverge rise to larger values. The maximum of the ZFC curve signalling T_B goes from 2.5 K at 0.01 K min^{-1} to 5 K at 5 K min^{-1} (Table S4‡). When increasing the field to 500 Oe, the blocking temperatures rise significantly; this is probably due to the suppression of relaxation through QTM. At very low heating rates (0.01 K min^{-1}), the blocking temperature is around 5 K and reaches 8 K at 2 K min^{-1}. Faster heating rates did not provide values for the blocking temperature since the ZFC curve had no clear maximum (see Figs. 2 and S6‡).

Alternating current (AC) magnetic susceptibility measurements were performed to study the slow relaxation of magnetisation. To obtain the maximum number of relaxation times and be able to study a larger temperature range, two pieces of equipment were employed to study the 1–10 000 Hz frequency range: SQUID MPMS XL and PPMS-9 instruments (see details in the ESI‡). At zero external DC field, the in-phase (χ'_M) and out-of-phase (χ''_M) components of the AC susceptibility show frequency-dependent peaks (Figs. S7 and S8‡) with well-defined maxima in the χ''_M *vs.* T plot over the 20–40 K range for higher frequencies (Fig. S8‡), indicating a high magnetisation reversal barrier. The χ''_M *vs.* frequency plot displays temperature-dependent maxima over the 19–27 K range (Fig. S9‡). The relaxation times were extracted from fitting of the frequency dependence of χ''_M at different temperatures using the generalized Debye model. The extracted relaxation times (τ) are collected in Table S5.‡

Magnetisation decay experiments were performed to evaluate relaxation times at lower temperatures. Exponential decay of the magnetisation was clearly observed until 8 K. The obtained data were fitted using a stretched exponential function (Fig. S11‡); this is commonly employed to obtain relaxation times from magnetisation decay measurements.[80,81] The obtained τ values are collected in Table S6‡ and represented in Fig. 3 as the $\ln(\tau^{-1})$ *vs.* temperature plot together with the obtained values from the AC susceptibility measurements. At very low temperature, there is a constant region indicative of quantum tunnelling relaxation. The onset of the Raman regime is discernible from magnetisation decay data, the trend in which matches with the lowest points measured by AC susceptibility. The transition between Raman and Orbach demagnetisation is clearly visible at around 18 K. As the three mag-

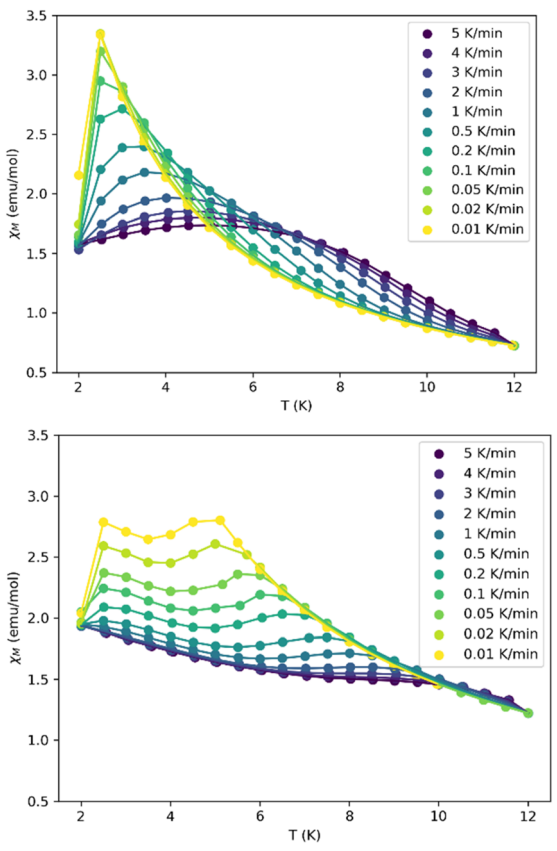

Fig. 2 Temperature dependence of χ_M under ZFC conditions at different heating rates and with an applied field of 50 Oe (above) and 500 Oe (below). FC data are omitted for a better appreciation of the ZFC curves and their dependence on the heating rate. ZFC/FC curves for all data are available as ESI (Fig. S5 and S6‡).

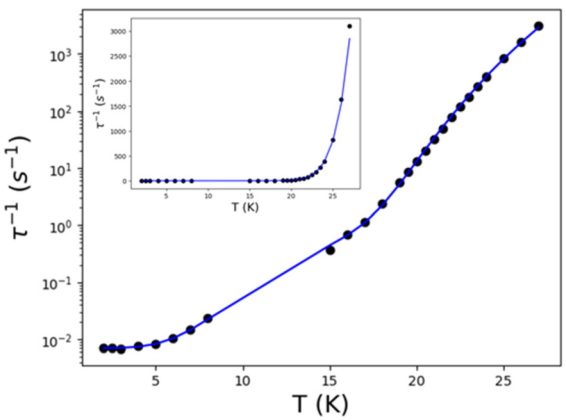

Fig. 3 Logarithmic plot of τ^{-1} *vs.* temperature for **1** (in the inset, τ^{-1} *vs.* temperature, as in eqn (14)). The values at lower temperatures correspond to those obtained from magnetisation decay and the values at higher temperatures are the ones derived from fitting of the AC susceptibility data to a generalized Debye function. The blue line corresponds to fitting of the data with eqn (14).

netic relaxation mechanisms are identified in the $\tau^{-1}(T)$ curve, the following equation is employed:

$$\tau^{-1} = {\tau_{\mathrm{QTM}}}^{-1} + CT^{n} + {\tau_0}^{-1}\mathrm{e}^{U_{\mathrm{eff}}/kT} \quad (14)$$

where the effective demagnetisation barrier was adjusted to a value of 427.7 K (297.3 cm^{-1}), with a preexponential factor (τ_0) of 4.66×10^{-11} s. Raman and tunnelling were fitted to $C = 2.64 \times 10^{-7}$ K^{-n} s^{-1}, $n = 5.28$ and $\tau_{\mathrm{QTM}} = 142.7$ s, respectively.

For completeness, the field dependent magnetisation measurements at different temperatures were acquired (Fig. 4), with a sweep rate of 20 mT s^{-1}. Compound **1** shows a clear magnetic hysteresis, which remains open up to 14 K; this is one of highest values for air/humidity stable SMMs synthesized to date. The butterfly shape of the hysteresis loop arises from a faster relaxation around zero field and a slower relaxation at intermediate fields. This compound retains a large magnetisation that falls only when $H < 20$ mT, which can be attributed to unsuppressed quantum tunnelling of the magnetisation due to symmetry deviation and hyperfine and dipole interactions. When the temperature increases, the hysteresis loop narrows as the relaxation speeds up and results in smaller coercive fields and remanent magnetisation. The hysteresis loop shows a coercive field of 1 T and a remanent magnetisation of $2\mu_{\mathrm{B}}$ at 3 K at a sweep rate of 20 mT s^{-1},

Ab initio calculations

Ab initio calculations based on the experimental X-ray structural data were performed to provide insights into the mechanism that governed the magnetic relaxation of complex **1**. In particular, multiconfigurational CASSCF calculations implemented in the ORCA 5.0.3 program package[82–84] and the CASSCF/RASSI-SO/SINGLE_ANISO approach using OpenMOLCAS[85–87] were carried out. Both programs agree in the general description of the double well potential associated with the ground $^6\mathrm{H}_{15/2}$ multiplet. To avoid redundancy in the discussion, we present the ORCA results in the manuscript while OpenMOLCAS data are presented in the ESI‡ for comparison.

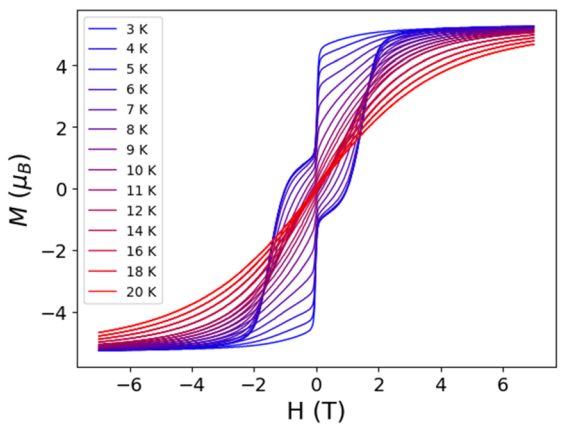

Fig. 4 Magnetic hysteresis measurements/hysteresis plot for **1** at a sweep rate of 20 mT s^{-1}.

The eight computed Kramers' doublets (KDs) for **1**, corresponding to the $^6\mathrm{H}_{15/2}$ ground state of the $\mathrm{Dy}^{\mathrm{III}}$ ion, span an energy range of about 674 cm^{-1} (Table S7‡). The computed temperature dependence of $\chi_{\mathrm{M}}T$ reproduces the experimental temperature dependence of $\chi_{\mathrm{M}}T$ rather well (Fig. S4‡). The ground KD (KD1) is a pure $m_J = |\pm 15/2\rangle$ state that is highly anisotropic ($g_{zz} = 19.86$) with negligible transverse components ($g_{xx} \sim g_{yy} < 1 \times 10^{-3}$), thus establishing a strong magnetic anisotropic axis. These *g*-values suggest strongly suppressed QTM within the ground KD (Fig. 5), which is consistent with the relatively large experimental value for τ_{QTM} (142.7 s). The anisotropic g_{zz} axis is almost collinear with the pseudo-C_5 axis lying along the axial O–Dy–O bonds (the deviation between the g_{zz} axis and O–Dy–O direction is 1.5°, see Fig. S12‡ and Fig. 5 bottom). This strong uniaxial magnetic anisotropy is consistent with the weak ligand field from aqua and bromine ligands in the equatorial plane and the strong donor ligands in the axial positions.

The first excited state (KD2) lies 275.2 cm^{-1} above the ground state. This KD2 is also axial in nature, with $g_{zz} = 16.92$, $g_{xx} = 0.13$, and $g_{yy} = 0.27$. In this case, the g_z tensor passes

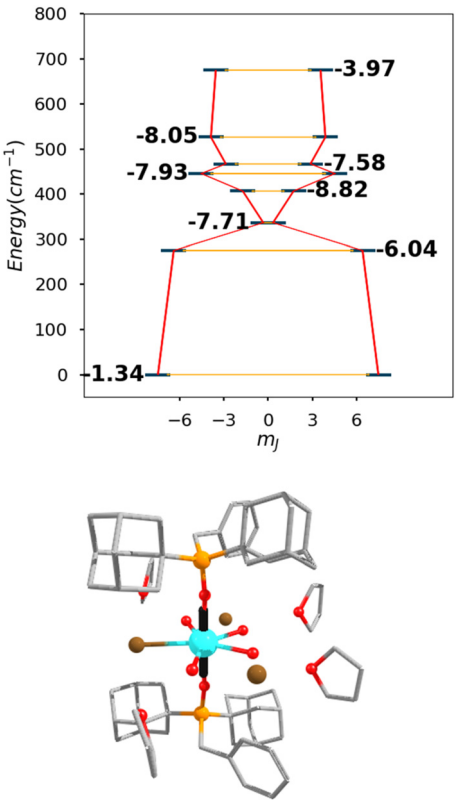

Fig. 5 Top: *ab initio* magnetisation blocking barrier for **1**, where the Kramers' doublets (KDs) are represented as dark blue bars and tunnelling relaxation times (τ_{QTM}) between the connecting pairs are indicated as orange lines and the values are represented on the $\log_{10}$ scale. Bottom: molecular structure of **1** with the calculated orientation of the main magnetic axis of the ground Kramers' doublet (KD1) (black line). Colour code: Dy (green), O (red), P (orange), Br (brown) and C (grey).

through the O–Dy–O direction again and presents a deviation of 6.4° with respect to the g_{zz} anisotropic axis of the ground state. The transverse components of KD2 can be large enough to promote magnetic relaxation *via* the first excited state, giving a calculated magnetisation barrier, U_{cal}, of 275.2 cm^{-1} (396 K), which is close to the experimental energy barrier, U_{eff}, of 427.7 K. The next excited state (KD3) is close in energy (336.6 cm^{-1}, 484 K) and shows large transverse components of g (g_{xx} = 0.42 and g_{yy} = 1.63). Tunnelling relaxation times were calculated according to an *ab initio* model based on the spin–dipolar interaction.[88] For the ground state (KD1), the calculated tunnelling time is 4.6×10^{-2} s while for the first excited state (KD2) it is much faster (9.1×10^{-7} s), which is consistent with the large transverse g-tensors obtained for the latter, confirming that magnetic relaxation for **1** occurs *via* the first excited state (KD2).

The effect of the f-orbital splitting on the observed magnetic anisotropy can be investigated in further detail by considering the individual contributions of each $f_{\pm n}$ orbital block to the demagnetisation barrier, as shown previously by some of us.[89] In the case of **1**, the high axiality of the coordination environment dictates orbital splitting where the most destabilized orbital corresponds to the f_0 (f_{z^3}) orbital, lying along the z-axis with an energy of 854 cm^{-1} (violet level in Fig. 6, top). Interestingly, the most stable orbital block is not the one lying on the xy plane ($f_{y(3x^2-y^2)}$ and $f_{x(x^2-3y^2)}$ orbitals, collectively named $f_{\pm 3}$) but the next block, the functions of which have a first-order dependency with respect to z (f_{xyz} and $f_{z(x^2-y^2)}$ orbitals, collectively named $f_{\pm 2}$) (red levels in Fig. 6, top). Fig. 6 (bottom) compares the CASSCF energies of the m_J sublevels of the ground $^6H_{15/2}$ multiplet with the ones derived from the orbital energies weighted by their contributions to each sublevel in a ligand field stabilization energy (LFSE) approach.[89] The agreement between both data sets is satisfactory as both present an isolated ground doublet, separated by *ca.* 300 cm^{-1} from a dense pack of seven doublets spanning around 300–400 cm^{-1}. The pattern of the double well resembles the letter "M", like the pattern derived from CASSCF (Fig. 5, top). Considering that magnetic relaxation probably proceeds *via* the first excited doublet, the contribution of each orbital block to anisotropy can be estimated from the LFSE energy difference between the m_j = ±13/2 and m_j = ±15/2 states, which is $2/3^*(E_{f_{\pm 1}} - E_{f_{\pm 2}})$. In this case, the average energy of the $f_{\pm 1}$ and $f_{\pm 2}$ orbital blocks is 9.5 cm^{-1} and 523.7 cm^{-1}, resulting in a gap of 342.8 cm^{-1}.

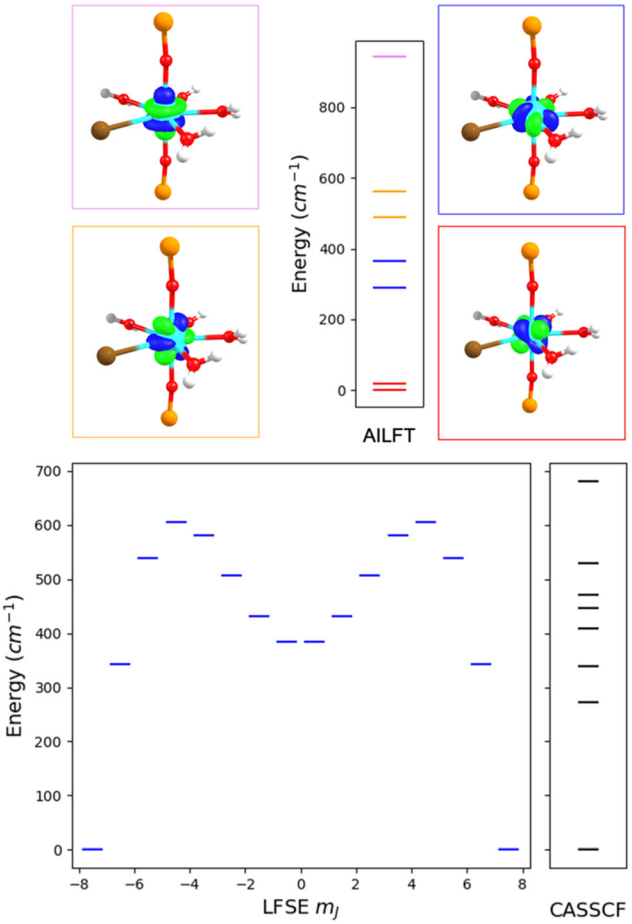

Fig. 6 Top: f-orbital energy splitting obtained from AILFT calculations; blue, red, orange, and violet levels correspond to $f_{\pm 3}$, $f_{\pm 2}$, $f_{\pm 1}$ and f_0 orbitals, respectively. One orbital for each block is depicted next to the corresponding level, where atoms not belonging to the immediate coordination environment of the Dy^{III} ion are omitted for clarity. Bottom: LFSE and CASSCF energy levels (in cm^{-1}) for **1** are represented in blue and black, respectively.

Model assessment

The accuracy of the presented model can be evaluated for **1** since the temperature dependence of the relaxation time successfully fits to the combination of tunnelling, Raman and Orbach contributions. Employing eqn (7), the ZFC curve can be simulated, and the maximum is obtained numerically. The effect of different demagnetisation mechanisms can be analysed by modifying the $\tau(T)$ curve to include diverse combinations of Orbach, tunnel, and Raman mechanisms. Our analysis starts with the ZFC/FC determined using a field of 500 Oe. At this field, the tunnelling mechanism should be mostly suppressed so only the Orbach and Raman mechanisms are considered in the integration of $\tau^{-1}(T)$. It is important to stress that the heating step in ZFC/FC measurements is done with an external magnetic field, which can affect demagnetisation parameters, especially tunnelling. Thus, care must be taken to account for this effect. Fig. 7 presents the simulated ZFC curves for all the experimentally determined heating rates (0.01–5 K min^{-1}). Pleasingly, the positions of the ZFC maxima are similar to the temperature range of the experiment (*vide supra*). In the same way as the analysis of the experimental ZFC/FC curves, data associated with the slower heating rates show ZFC curves where $T_{B\text{-}ZFC/FC}$ is clearly discernible, while the faster heating rates show a less clear maximum.

The former simulations are now repeated by incorporating tunnelling relaxation into the integration of $\tau^{-1}(T)$. The reference experimental data are now in the ZFC/FC curve measured at 50 Oe, which should present a smaller quenching of tunnel-

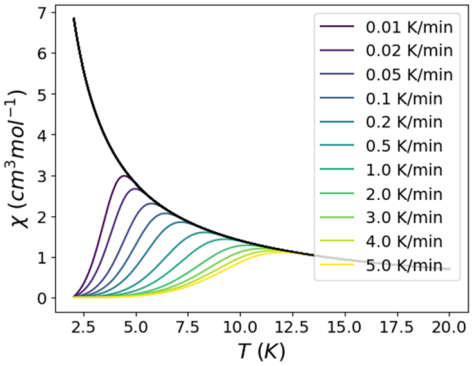

Fig. 7 Simulated ZFC/FC curve for the sum of the Orbach and Raman mechanisms, using the demagnetisation parameters fitted for **1**. C_1' is assumed to be one and the adiabatic susceptibility is represented in black with a fixed value of χ_T = 14.17 cm^3 K mol^{-1}.

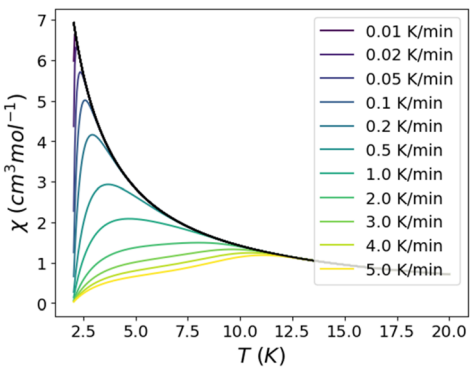

Fig. 8 Simulated ZFC/FC curve for the sum of tunnelling, Orbach and Raman mechanisms, using the demagnetisation parameters fitted for *z*. C_1' is assumed to be one and the adiabatic susceptibility is represented in black with a fixed value of χ_T = 14.17 cm^3 K mol^{-1}.

ling than the 500 Oe results. Fig. 8 shows the simulated curves under these conditions. The comparison between Fig. 7 and 8 clearly indicates that tunnelling is efficient at lowering $T_{B\text{-}ZFC/FC}$ for **1**, in the same way that ZFC/FC data at 500 Oe show higher blocking temperatures than the 50 Oe results. This highlights an important and probably overlooked experimental parameter that affects the blocking temperatures measured by ZFC/FC experiments: the external field necessary to record the magnetic moment along the temperature program, which adds to the importance of reporting the heating rate for these experiments.

A more quantitative comparison between the experimental and calculated blocking temperatures is presented in Fig. 9. As mentioned earlier, the model can capture the effect of tunnelling in **1**, which diminishes the blocking temperature by around 5 K. The agreement is quantitative at low heating rates but departs for faster heating rates (see the red dashed line in Fig. 9). Small modifications to the tunnelling value reveal a high sensitivity of the blocking temperature, where correcting the tunnelling time by a factor of 0.25 provides a simulated

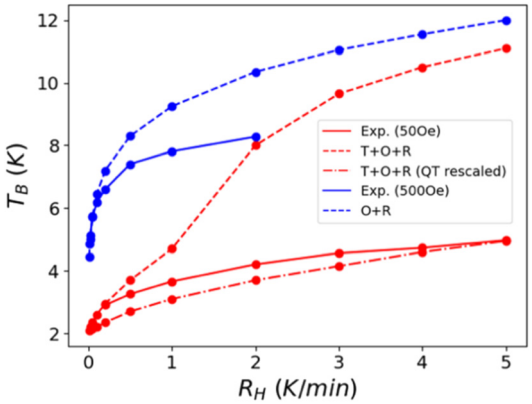

Fig. 9 Comparison of experimental (solid lines) and simulated (dashed or dotted–dashed lines) blocking temperatures. Data corresponding to 50 Oe and 500 Oe measurements are depicted in red and blue, respectively.

curve that agrees with the 50 Oe experiment over the complete range of heating rates (dotted–dashed red line in Fig. 9). This factor might seem a drastic correction, but it is significantly lower than the error bars of the magnetisation decay measurements calculated from the β parameter, according to Chilton and coworkers.[90] In this case, the range of relaxation times is even larger since the magnetisation decay and AC susceptibility are combined. The 500 Oe data also agree with simulations, where the low heating rate results agree perfectly and depart by a couple of K at faster rates. Overall, the performance of the model is satisfactory since it allows us to predict $T_{B\text{-}ZFC/FC}$ accurately and capture the heating rate dependency.

The demagnetisation mechanism limiting the blocking temperature can be estimated by repeating the same simulations and including each demagnetisation mechanism separately. The tunnelling mechanism limits T_B to 2–3 K for slow heating rates while it keeps most of the magnetic moment frozen at faster temperature programs, without reaching a maximum over the simulated temperature range (2–20 K) (see Fig. S14,‡ left). The Raman-only simulation is similar to the one for the Orbach + Raman results from Fig. 8, indicating that Raman relaxation is responsible for the simulated blocking between 4 and 12 K. The Orbach-only plot shows blocking temperatures over a higher temperature range (14–17 K). Hence, it does not determine the value of T_B in this case (see Fig. S14,‡ right).

To assess the broader accuracy of the presented approach, a literature search for experimental examples of $T_{B\text{-}ZFC/FC}$ was performed. Such values can also be obtained for any single-molecule magnet system by introducing the spin relaxation parameters at the web page **https://tbsim.ee.ub.edu**. By reconstructing the $\tau(T)$ curve using fitting parameters, we can calculate T_B using eqn (7). Unfortunately, the heating rate is not always reported, so we have assumed lower and higher limit values for this parameter when R_H information is missing (0.2 K min^{-1} and 5 K min^{-1} to account for slow and fast sweeping rates).

Table S9‡ compares experimental and predicted values for ZFC/FC blocking temperatures for 97 lanthanide SMMs[13,14,37,38,41,50,51,60,61,63,65,91–136] and ten transition metal complexes[137–146] reported in the literature. The lanthanide benchmark set contains mononuclear and polynuclear complexes based on Dy^{III}, Tb^{III}, Er^{III} and Ho^{III} ions, heteronuclear complexes containing Dy^{III} or Tb^{III} ions and transition metals, including diluted systems. The ten transition compounds are Mn_{12} complexes, a trinuclear Mn_2Mo complex, and tetranuclear and mononuclear iron and cobalt complexes. The fitting parameters for AC susceptibility data range from systems involving combinations of Orbach, Raman, and tunnelling, Orbach and Raman, Orbach and tunnelling, and Raman and tunnelling to Orbach-only terms. Besides, the list includes complexes exhibiting two or three relaxation processes, where one of them (the main process) is considered to calculate T_B. As observed in this list, some authors report T_{irrev} (indicated with an asterisk) instead $T_{B\text{-}ZFC/FC}$, and others report both values. As expected, T_{irrev} is always higher than the $T_{B\text{-}ZFC/FC}$ value. In some cases, the difference between T_{irrev} and $T_{B\text{-}ZFC/FC}$ values exceeds 10 K (*e.g.* 78 K and ~55 K, respectively, for complex **3** in Table S9‡). Another issue to highlight is the lack of information about the heating rate (R_H). From the 107 complexes in Table S9,‡ R_H values were only included in the original papers for 37 systems, and only for 3 transition metal complexes (see Fig. 10). Reported R_H values range from 0.189 to 5 K min^{-1}, demonstrating that there is no consensus on this important parameter that defines the T_B value. In most cases, the reported $T_{B\text{-}ZFC/FC}$ value lies in the range of T_B obtained with R_H values of 0.2 K min^{-1} and 5 K min^{-1}, or close to these values (see Fig. 11). Similarly, when R_H is reported, the obtained T_B value at this heating rate is close to the reported $T_{B\text{-}ZFC/FC}$ value (see Fig. 10), demonstrating the accuracy and broad applicability of the presented approach.

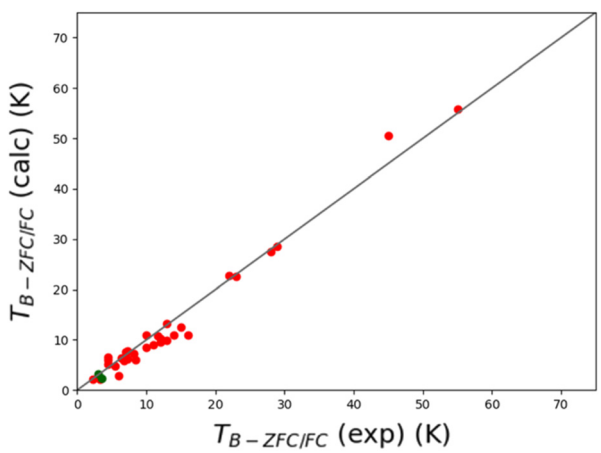

Fig. 10 Comparison of the experimental zero-field cooling/field cooling blocking temperatures and the ones calculated using eqn (12). Only 38 cases (35 lanthanide and 3 transition metal compounds depicted in red and green, respectively) with a reported heating rate are considered (see Fig. 11 for the other systems). The black line represents perfect agreement between both values.

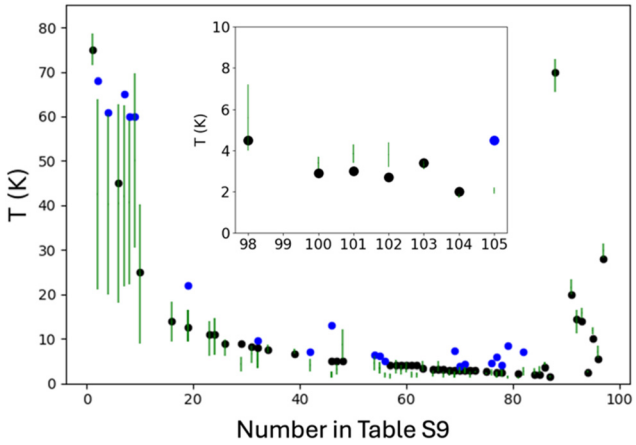

Fig. 11 Comparison of the experimental $T_{B\text{-}ZFC/FC}$ blocking (black dots) or T_{irrev} irreversible (blue dots, values in Table S9‡ indicated with an asterisk) temperatures for the 62 lanthanide systems (for clarity, the 7 transition metal systems are in the inset) without a reported heating rate. The *x*-axis indicates the complex number in Table S9.‡ The green bar corresponds to the limit values calculated using eqn (12) using with R_H = 0.2 K min^{-1} and 5 K min^{-1}.

The large amount of data collected in Table S9‡ allow us to investigate if a temperature at a fixed relaxation time like $T_{B\text{-}100}$ can be useful as a descriptor for ZFC/FC blocking temperatures. Fig. S15‡ presents the relaxation time at the experimental $T_{B\text{-}ZFC/FC}$ value for the data presented in Table S9‡ as a function of the heating rate. Clusters of data are observed around the most common R_H values (0.2–0.4 K min^{-1}, 2 K min^{-1} and 5 K min^{-1}). In all cases, a high dispersion of relaxation times at the experimental $T_{B\text{-}ZFC/FC}$ value is observed, especially for slow heating rates. In the case of the cluster located at 0.2–0.4 K min^{-1}, the maximum and minimum relaxation times are 282 s and 1 s. Thus, the experimental $T_{B\text{-}ZFC/FC}$ value cannot be related with a unique treshold value of the relaxation time, even at a fixed heating rate.

For systems without a reported heating rate, the limiting values of the blocking temperature were calculated considering R_H values of 0.2 K min^{-1} and 5 K min^{-1}, as shown in Fig. 11. In practically all cases, the $T_{B\text{-}ZFC/FC}$ value falls within the calculated range. Furthermore, the T_{irrev} values tend to appear in the highest part or above the bars associated with the limiting R_H values, in agreement with the fact that the irreversibility temperature (T_{irrev}) must be higher than $T_{B\text{-}ZFC/FC}$.[78]

Conclusions

This work discusses the various metrics for quantifying blocking temperatures and the challenges associated with each method. The newly proposed approach for estimating $T_{B\text{-}ZFC/FC}$ from AC susceptibility parameters offers a practical way to compare the performance of SMMs in the literature and estimate $T_{B\text{-}ZFC/FC}$ without the need for additional measurements. Thus, the $T_{B\text{-}ZFC/FC}$ blocking temperature for a given heating rate can be estimated from the relaxation time data, which are

the most common magnetic characterization data available for SMMs. In this context, the synthesis and characterization of the Dy^{III} SMM with D_{5h} geometry, $[Dy(OPAd_2Bz)_2(H_2O)_4Br]Br_2{\cdot}4THF$ (**1**), enabled the predictions of the blocking temperature to be tested over a broad range of heating rates and two different static magnetic fields. Furthermore, complex **1** is an interesting example of an air- and humidity-stable SMM with high U_{eff} and T_B values, adding to the restricted list of examples of SMMs with D_{5h} geometry.

Magnetic measurements confirm the SMM behaviour of complex **1**, with a ZFC/FC blocking temperature in the range of 2.5–8 K, depending on the heating rate and the magnitude of the probe magnetic field. The presence of the magnetic hysteresis at zero-field with a large coercive field and remanent magnetisation values further supports the SMM properties of the complex. Additionally, AC magnetic susceptibility measurements reveal a high magnetisation reversal barrier, indicating slow relaxation of magnetisation. *Ab initio* calculations provide insights into the electronic structure and relaxation mechanism of complex **1**. The calculations confirm the strong uniaxial magnetic anisotropy and reveal that magnetic relaxation occurs primarily *via* the first excited state (KD2).

In summary, the study of complex **1** exemplifies the potential of stable SMMs with D_{5h} geometry and axial ligands for achieving high-performance SMMs. The proposed approach for estimating $T_{B\text{-}ZFC/FC}$ provided accurate values of the ZFC/FC blocking temperature of **1**, properly captured the heating rate and probe field dependence of $T_{B\text{-}ZFC/FC}$ and highlighted their importance. The study also identified the Raman and tunnelling mechanisms as the ones determining the blocking temperature. The possibility of relating the spin relaxation mechanisms directly to the blocking temperature opens the way for a better understanding of T_B tuning, which is a fundamental parameter of SMMs. Furthermore, the proposal successfully predicted blocking temperatures for many examples of SMMs in the literature, offering a valuable tool for characterising and comparing SMMs in future research.

Author contributions

Y. G. and M. A. P.: investigation, data analysis; D. A.: software; M. M. Q. M., E. C., S. G. C., E. R. and D. A.: conceptualisation, investigation, data analysis, validation, supervision, resources, funding acquisition; all authors contributed to the writing and editing of the article.

Data availability

The data supporting this article have been included as part of the ESI.‡ Estimation of the blocking temperature for any single-molecule magnet system can be obtained by introducing the spin relaxation parameters at the web page **https://tbsim.ee.ub.edu**.

Conflicts of interest

There are no conflicts to declare.

Acknowledgements

D. A. thanks FONDECYT Regular 1210325 for financial support. Powered@NLHPC: this research was partially supported by the supercomputing infrastructure of the NLHPC (ECM-02). Financial support from the Ministerio de Ciencia e Innovación (projects PID2022-138090NB-C21, PID2021-122464NB-I00, TED2021-129593B-I00, CNS2023-144561 and Maria de Maeztu CEX2021-001202-M), the Junta de Andalucía (FQM-195 and FQM-337), FEDER/Junta de Andalucía (projects I + D + i P20_00692, C-EXP-140-UGR23 and M.1.B.B TA_000722, Programas Operativos FEDER 2014-2020 y 2021-2027, Consejería de Economía, Conocimiento, Empresas y Universidad), and the University of Granada (project I + D + i PPJIA2020.10) is greatly appreciated. The authors also acknowledge the Centro de Servicios de Informática y Redes de Comunicaciones (CSIRC) for computational time and facilities. M.M.Q.M. thanks the Ministerio de Ciencia e Innovación for a Ramón y Cajal contract (the publication is part of the project PID2022-138090NB-C21 and grant RYC2021-034288-I funded by MCIN/AEI/10.13039/501100011033 and by the European Union "NextGenerationEU"/PRTR"). E. R. also acknowledges the Generalitat de Catalunya for ICREA Academia and 2021-SGR-00286 grants, and for computational resources at CSUC.

References

1 S. M. J. Aubin, M. W. Wemple, D. M. Adams, H.-L. Tsai, G. Christou and D. N. Hendrickson, Distorted MnIVMnIII$_3$ Cubane Complexes as Single-Molecule Magnets, *J. Am. Chem. Soc.*, 1996, **118**, 7746–7754.
2 R. Sessoli, D. Gatteschi, A. Caneschi and M. A. Novak, Magnetic bistability in a metal-ion cluster, *Nature*, 1993, **365**, 141–143.
3 D. N. Woodruff, R. E. P. Winpenny and R. A. Layfield, Lanthanide Single-Molecule Magnets, *Chem. Rev.*, 2013, **113**, 5110–5148.
4 A. Zabala-Lekuona, J. M. Seco and E. Colacio, Single-Molecule Magnets: From Mn_{12}-ac to dysprosium metallocenes, a travel in time, *Coord. Chem. Rev.*, 2021, **441**, 213984.
5 N. F. Chilton, Molecular Magnetism, *Annu. Rev. Mater. Res.*, 2022, **52**, 79–101.
6 E. Coronado, Molecular magnetism: from chemical design to spin control in molecules, materials and devices, *Nat. Rev. Mater.*, 2019, **5**, 87–104.
7 A. Gaita-Ariño, F. Luis, S. Hill and E. Coronado, Molecular spins for quantum computation, *Nat. Chem.*, 2019, **11**, 301–309.

8 J. Long, Y. Guari, R. A. S. Ferreira, L. D. Carlos and J. Larionova, Recent advances in luminescent lanthanide based Single-Molecule Magnets, *Coord. Chem. Rev.*, 2018, **363**, 57–70.
9 R. Marin, G. Brunet and M. Murugesu, Shining New Light on Multifunctional Lanthanide Single–Molecule Magnets, *Angew. Chem., Int. Ed.*, 2020, **60**, 1728–1746.
10 E. Moreno-Pineda and W. Wernsdorfer, Measuring molecular magnets for quantum technologies, *Nat. Rev. Phys.*, 2021, **3**, 645–659.
11 M. Shiddiq, D. Komijani, Y. Duan, A. Gaita-Ariño, E. Coronado and S. Hill, Enhancing coherence in molecular spin qubits via atomic clock transitions, *Nature*, 2016, **531**, 348–351.
12 R. Vincent, S. Klyatskaya, M. Ruben, W. Wernsdorfer and F. Balestro, Electronic read-out of a single nuclear spin using a molecular spin transistor, *Nature*, 2012, **488**, 357–360.
13 F. Liu, D. S. Krylov, L. Spree, S. M. Avdoshenko, N. A. Samoylova, M. Rosenkranz, A. Kostanyan, T. Greber, A. U. B. Wolter, B. Büchner and A. A. Popov, Single molecule magnet with an unpaired electron trapped between two lanthanide ions inside a fullerene, *Nat. Commun.*, 2017, **8**, 16098.
14 F. Liu, G. Velkos, D. S. Krylov, L. Spree, M. Zalibera, R. Ray, N. A. Samoylova, C.-H. Chen, M. Rosenkranz, S. Schiemenz, F. Ziegs, K. Nenkov, A. Kostanyan, T. Greber, A. U. B. Wolter, M. Richter, B. Büchner, S. M. Avdoshenko and A. A. Popov, Air-stable redox-active nanomagnets with lanthanide spins radical-bridged by a metal–metal bond, *Nat. Commun.*, 2019, **10**, 571.
15 B. M. Day, F.-S. Guo and R. A. Layfield, Cyclopentadienyl Ligands in Lanthanide Single-Molecule Magnets: One Ring To Rule Them All?, *Acc. Chem. Res.*, 2018, **51**, 1880–1889.
16 A. Dey, P. Kalita and V. Chandrasekhar, Lanthanide(III)-Based Single-Ion Magnets, *ACS Omega*, 2018, **3**, 9462–9475.
17 K. L. M. Harriman and M. Murugesu, An Organolanthanide Building Block Approach to Single-Molecule Magnets, *Acc. Chem. Res.*, 2016, **49**, 1158–1167.
18 J.-L. Liu, Y.-C. Chen and M.-L. Tong, Symmetry strategies for high performance lanthanide-based single-molecule magnets, *Chem. Soc. Rev.*, 2018, **47**, 2431–2453.
19 J. Tang and P. Zhang, Dinuclear Lanthanide Single-Molecule Magnets, in *Lanthanide Single Molecule Magnets*, Springer Berlin Heidelberg, 2015, pp. 91–126.
20 J. Wang, C. Y. Sun, Q. Zheng, D. Q. Wang, Y. T. Chen, J. F. Ju, T. M. Sun, Y. Cui, Y. Ding and Y. F. Tang, Lanthanide Single–molecule Magnets: Synthetic Strategy, Structures, Properties and Recent Advances, *Chem. – Asian J.*, 2023, **18**, e202201297.
21 A. J. Brown, D. Pinkowicz, M. R. Saber and K. R. Dunbar, A Trigonal-Pyramidal Erbium(III) Single-Molecule Magnet, *Angew. Chem., Int. Ed.*, 2015, **54**, 5864–5868.
22 Y. Chen, F. Ma, X. Chen, B. Dong, K. Wang, S. Jiang, C. Wang, X. Chen, D. Qi, H. Sun, B. Wang, S. Gao and J. Jiang, A New Bis(phthalocyaninato) Terbium Single-Ion Magnet with an Overall Excellent Magnetic Performance, *Inorg. Chem.*, 2017, **56**, 13889–13896.
23 C. R. Ganivet, B. Ballesteros, G. de la Torre, J. M. Clemente-Juan, E. Coronado and T. Torres, Influence of Peripheral Substitution on the Magnetic Behavior of Single-Ion Magnets Based on Homo- and Heteroleptic TbIII Bis(phthalocyaninate), *Chem. – Eur. J.*, 2013, **19**, 1457–1465.
24 N. Ishikawa, M. Sugita, N. Tanaka, T. Ishikawa, S.-y. Koshihara and Y. Kaizu, Upward Temperature Shift of the Intrinsic Phase Lag of the Magnetization of Bis(phthalocyaninato)terbium by Ligand Oxidation Creating an S = 1/2 Spin, *Inorg. Chem.*, 2004, **43**, 5498–5500.
25 W.-J. Xu, Q.-C. Luo, Z.-H. Li, Y.-Q. Zhai and Y.-Z. Zheng, Bis-Alkoxide Dysprosium(III) Crown Ether Complexes Exhibit Tunable Air Stability and Record Energy Barrier, *Adv. Sci.*, 2024, **11**, 2308548.
26 Z.-H. Li, Y.-Q. Zhai, W.-P. Chen, Y.-S. Ding and Y.-Z. Zheng, Air-Stable Hexagonal Bipyramidal Dysprosium(III) Single-Ion Magnets with Nearly Perfect D_{6h} Local Symmetry, *Chem. – Eur. J.*, 2019, **25**, 16219–16224.
27 F. Benner, L. La Droitte, O. Cador, B. Le Guennic and S. Demir, Magnetic hysteresis and large coercivity in bis-benzimidazole radical-bridged dilanthanide complexes, *Chem. Sci.*, 2023, **14**, 5577–5592.
28 J. Tang, I. Hewitt, N. T. Madhu, G. Chastanet, W. Wernsdorfer, C. E. Anson, C. Benelli, R. Sessoli and A. K. Powell, Dysprosium Triangles Showing Single-Molecule Magnet Behavior of Thermally Excited Spin States, *Angew. Chem., Int. Ed.*, 2006, **45**, 1729–1733.
29 P. Zhang, F. Benner, N. F. Chilton and S. Demir, Organometallic lanthanide bismuth cluster single-molecule magnets, *Chem*, 2022, **8**, 717–730.
30 N. F. Chilton, C. A. P. Goodwin, D. P. Mills and R. E. P. Winpenny, The first near-linear bis(amide) f-block complex: a blueprint for a high temperature single molecule magnet, *Chem. Commun.*, 2015, **51**, 101–103.
31 J. D. Rinehart and J. R. Long, Exploiting single-ion anisotropy in the design of f-element single-molecule magnets, *Chem. Sci.*, 2011, **2**, 2078.
32 L. Ungur and L. F. Chibotaru, Strategies toward High-Temperature Lanthanide-Based Single-Molecule Magnets, *Inorg. Chem.*, 2016, **55**, 10043–10056.
33 S. Dey, T. Sharma and G. Rajaraman, Unravelling the role of spin–vibrational coupling in designing high-performance pentagonal bipyramidal Dy(iii) single ion magnets, *Chem. Sci.*, 2024, **15**, 6465–6477.
34 S. Mondal and A. Lunghi, Unraveling the Contributions to Spin–Lattice Relaxation in Kramers Single-Molecule Magnets, *J. Am. Chem. Soc.*, 2022, **144**, 22965–22975.
35 V. Vieru, S. Gómez-Coca, E. Ruiz and L. F. Chibotaru, Increasing the Magnetic Blocking Temperature of Single-Molecule Magnets, *Angew. Chem., Int. Ed.*, 2024, **63**, e202303146.

36 T. Sharma, A. Swain and G. Rajaraman, Pushing Boundaries in Single Molecule Magnets: An Ab Initio Perspective on Harnessing Unusual Oxidation States for Unprecedented Lanthanide SMM Performance, *ChemRxiv*, 2023. DOI: 10.26434/chemrxiv-2023-wpc4r.

37 F.-S. Guo, B. M. Day, Y.-C. Chen, M.-L. Tong, A. Mansikkamäki and R. A. Layfield, Magnetic hysteresis up to 80 kelvin in a dysprosium metallocene single-molecule magnet, *Science*, 2018, **362**, 1400–1403.

38 C. A. Gould, K. R. McClain, D. Reta, J. G. C. Kragskow, D. A. Marchiori, E. Lachman, E.-S. Choi, J. G. Analytis, R. D. Britt, N. F. Chilton, B. G. Harvey and J. R. Long, Ultrahard magnetism from mixed-valence dilanthanide complexes with metal-metal bonding, *Science*, 2022, **375**, 198–202.

39 D. Aravena and E. Ruiz, Shedding Light on the Single-Molecule Magnet Behavior of Mononuclear DyIII Complexes, *Inorg. Chem.*, 2013, **52**, 13770–13778.

40 N. F. Chilton, D. Collison, E. J. L. McInnes, R. E. P. Winpenny and A. Soncini, An electrostatic model for the determination of magnetic anisotropy in dysprosium complexes, *Nat. Commun.*, 2013, **4**, 3551.

41 M. Gregson, N. F. Chilton, A.-M. Ariciu, F. Tuna, I. F. Crowe, W. Lewis, A. J. Blake, D. Collison, E. J. L. McInnes, R. E. P. Winpenny and S. T. Liddle, A monometallic lanthanide bis(methanediide) single molecule magnet with a large energy barrier and complex spin relaxation behaviour, *Chem. Sci.*, 2016, **7**, 155–165.

42 S. T. Liddle and J. van Slageren, Improving f-element single molecule magnets, *Chem. Soc. Rev.*, 2015, **44**, 6655–6669.

43 K. L. M. Harriman, J. L. Brosmer, L. Ungur, P. L. Diaconescu and M. Murugesu, Pursuit of Record Breaking Energy Barriers: A Study of Magnetic Axiality in Diamide Ligated DyIII Single-Molecule Magnets, *J. Am. Chem. Soc.*, 2017, **139**, 1420–1423.

44 P. Zhang, L. Zhang, C. Wang, S. Xue, S.-Y. Lin and J. Tang, Equatorially Coordinated Lanthanide Single Ion Magnets, *J. Am. Chem. Soc.*, 2014, **136**, 4484–4487.

45 M. A. AlDamen, J. M. Clemente-Juan, E. Coronado, C. Martí-Gastaldo and A. Gaita-Ariño, Mononuclear Lanthanide Single-Molecule Magnets Based on Polyoxometalates, *J. Am. Chem. Soc.*, 2008, **130**, 8874–8875.

46 P.-E. Car, M. Perfetti, M. Mannini, A. Favre, A. Caneschi and R. Sessoli, Giant field dependence of the low temperature relaxation of the magnetization in a dysprosium(III)–DOTA complex, *Chem. Commun.*, 2011, **47**, 3751.

47 K. Katoh, S. Yamashita, N. Yasuda, Y. Kitagawa, B. K. Breedlove, Y. Nakazawa and M. Yamashita, Frontispiece: Control of the Spin Dynamics of Single-Molecule Magnets by using a Quasi One-Dimensional Arrangement, *Angew. Chem., Int. Ed.*, 2018, **57**, 9262–9267.

48 L. Sorace, C. Benelli and D. Gatteschi, Lanthanides in molecular magnetism: old tools in a new field, *Chem. Soc. Rev.*, 2011, **40**, 3092–3104.

49 A. M. Atkin, M. J. Giansiracusa, S. Calvello, E. Rousset, R. W. Gable, W. Phonsri, K. S. Murray, J. K. Howard, A. Soncini, R. A. Mole and C. Boskovic, bis(2,2′-bipyridine)-(methanol)-[3,4,5,6-tetrabromobenzene-1,2-diolato]-(3,4,5,6 tetrabromobenzene-1,2-diolato)-dysprosium(III), *Inorg. Chem.*, 2023, **62**, 1141.

50 C. A. P. Goodwin, F. Ortu, D. Reta, N. F. Chilton and D. P. Mills, Molecular magnetic hysteresis at 60 kelvin in dysprosocenium, *Nature*, 2017, **548**, 439–442.

51 F.-S. Guo, B. M. Day, Y.-C. Chen, M.-L. Tong, A. Mansikkamäki and R. A. Layfield, A Dysprosium Metallocene Single-Molecule Magnet Functioning at the Axial Limit, *Angew. Chem., Int. Ed.*, 2017, **56**, 11445–11449.

52 S.-D. Jiang, B.-W. Wang, H.-L. Sun, Z.-M. Wang and S. Gao, An Organometallic Single-Ion Magnet, *J. Am. Chem. Soc.*, 2011, **133**, 4730–4733.

53 L. Münzfeld, C. Schoo, S. Bestgen, E. Moreno-Pineda, R. Köppe, M. Ruben and P. W. Roesky, Synthesis, structures and magnetic properties of $[(\eta_9\text{-}C_9H_9)Ln(\eta_8\text{-}C_8H_8)]$ super sandwich complexes, *Nat. Commun.*, 2019, **10**, 3135.

54 A. H. Vincent, Y. L. Whyatt, N. F. Chilton and J. R. Long, Strong Axiality in a Dysprosium(III) Bis(borolide) Complex Leads to Magnetic Blocking at 65 K, *J. Am. Chem. Soc.*, 2023, **145**, 1572–1579.

55 A. B. Canaj, S. Dey, C. Wilson, O. Céspedes, G. Rajaraman and M. Murrie, Engineering macrocyclic high performance pentagonal bipyramidal Dy(iii) single-ion magnets, *Chem. Commun.*, 2020, **56**, 12037–12040.

56 A. B. Canaj, M. K. Singh, C. Wilson, G. Rajaraman and M. Murrie, Chemical and *in silico* tuning of the magnetisation reversal barrier in pentagonal bipyramidal Dy(iii) single-ion magnets, *Chem. Commun.*, 2018, **54**, 8273–8276.

57 Y.-C. Chen, J.-L. Liu, Y. Lan, Z.-Q. Zhong, A. Mansikkamäki, L. Ungur, Q.-W. Li, J.-H. Jia, L. F. Chibotaru, J.-B. Han, W. Wernsdorfer, X.-M. Chen and M.-L. Tong, Dynamic Magnetic and Optical Insight into a High-Performance Pentagonal Bipyramidal DyIII Single-Ion Magnet, *Chem. – Eur. J.*, 2017, **23**, 5630–5630.

58 Y.-C. Chen, J.-L. Liu, L. Ungur, J. Liu, Q.-W. Li, L.-F. Wang, Z.-P. Ni, L. F. Chibotaru, X.-M. Chen and M.-L. Tong, Symmetry-Supported Magnetic Blocking at 20 K in Pentagonal Bipyramidal Dy(III) Single-Ion Magnets, *J. Am. Chem. Soc.*, 2016, **138**, 2829–2837.

59 I. F. Díaz-Ortega, J. M. Herrera, S. Dey, H. Nojiri, G. Rajaraman and E. Colacio, The effect of the electronic structure and flexibility of the counteranions on magnetization relaxation in $[Dy(L)_2(H_2O)_5]^{3+}$ (L = phosphine oxide derivative) pentagonal bipyramidal SIMs, *Inorg. Chem. Front.*, 2020, **7**, 689–699.

60 Y.-S. Ding, N. F. Chilton, R. E. P. Winpenny and Y.-Z. Zheng, On Approaching the Limit of Molecular Magnetic Anisotropy: A Near-Perfect Pentagonal Bipyramidal Dysprosium(III) Single-Molecule Magnet, *Angew. Chem., Int. Ed.*, 2016, **55**, 16071–16074.

61 Y. S. Ding, T. Han, Y. Q. Zhai, D. Reta, N. F. Chilton, R. E. P. Winpenny and Y. Z. Zheng, A Study of Magnetic Relaxation in Dysprosium(III) Single–Molecule Magnets, *Chem. – Eur. J.*, 2020, **26**, 5893–5902.

62 S. K. Gupta, T. Rajeshkumar, G. Rajaraman and R. Murugavel, An air-stable Dy(iii) single-ion magnet with high anisotropy barrier and blocking temperature, *Chem. Sci.*, 2016, **7**, 5181–5191.

63 Z. Jiang, L. Sun, Q. Yang, B. Yin, H. Ke, J. Han, Q. Wei, G. Xie and S. Chen, Excess axial electrostatic repulsion as a criterion for pentagonal bipyramidal DyIII single-ion magnets with high U_{eff} and TB, *J. Mater. Chem. C*, 2018, **6**, 4273–4280.

64 L.-L. Li, H.-D. Su, S. Liu, Y.-C. Xu and W.-Z. Wang, A new air- and moisture-stable pentagonal-bipyramidal DyIII single-ion magnet based on the HMPA ligand, *Dalton Trans.*, 2019, **48**, 2213–2219.

65 J. Liu, Y.-C. Chen, J.-L. Liu, V. Vieru, L. Ungur, J.-H. Jia, L. F. Chibotaru, Y. Lan, W. Wernsdorfer, S. Gao, X.-M. Chen and M.-L. Tong, A Stable Pentagonal Bipyramidal Dy(III) Single-Ion Magnet with a Record Magnetization Reversal Barrier over 1000 K, *J. Am. Chem. Soc.*, 2016, **138**, 5441–5450.

66 J.-L. Liu, Y.-C. Chen, Y.-Z. Zheng, W.-Q. Lin, L. Ungur, W. Wernsdorfer, L. F. Chibotaru and M.-L. Tong, Switching the anisotropy barrier of a single-ion magnet by symmetry change from quasi-D_{5h} to quasi-O_h, *Chem. Sci.*, 2013, **4**, 3310.

67 J. Long, A. N. Selikhov, E. Mamontova, K. A. Lyssenko, Y. Guari, J. Larionova and A. A. Trifonov, Single-molecule magnet behaviour in a Dy(iii) pentagonal bipyramidal complex with a quasi-linear Cl–Dy–Cl sequence, *Dalton Trans.*, 2019, **48**, 35–39.

68 H. Wu, M. Li, B. Yin, Z. Xia, H. Ke, Q. Wei, G. Xie, S. Chen and S. Gao, Fine-tuning the type of equatorial donor atom in pentagonal bipyramidal Dy(iii) complexes to enhance single-molecule magnet properties, *Dalton Trans.*, 2019, **48**, 16384–16394.

69 B. Zhang, X. Guo, P. Tan, W. Lv, X. Bai, Y. Zhou, A. Yuan, L. Chen, D. Liu, H.-H. Cui, R. Wang and X.-T. Chen, Axial Ligand as a Critical Factor for High-Performance Pentagonal Bipyramidal Dy(III) Single-Ion Magnets, *Inorg. Chem.*, 2022, **61**, 19726–19734.

70 L. Zhu, Y. Dong, B. Yin, P. Ma and D. Li, Improving the single-molecule magnet properties of two pentagonal bipyramidal Dy^{3+} compounds by the introduction of both electron-withdrawing and -donating groups, *Dalton Trans.*, 2021, **50**, 12607–12618.

71 Y. Ma, Y.-Q. Zhai, Q.-C. Luo, Y.-S. Ding and Y.-Z. Zheng, Ligand Fluorination to Mitigate the Raman Relaxation of DyIII Single-Molecule Magnets: A Combined Terahertz, Far-IR and Vibronic Barrier Model Study, *Angew. Chem., Int. Ed.*, 2022, **61**, e202206022.

72 X. Ding, Q. Luo, Y. Zhai, X. Zhang, Y. Lv, X. Zhang, C. Ke, C. Wu and Y. Zheng, Rigid Dysprosium(III) Single-Molecule Magnets Exhibit Preserved Superparamagnetism in Solution, *Chin. J. Chem.*, 2022, **40**, 563–570.

73 K.-X. Yu, Y.-S. Ding, Y.-Q. Zhai, T. Han and Y.-Z. Zheng, Equatorial coordination optimization for enhanced axiality of mononuclear Dy(iii) single-molecule magnets, *Dalton Trans.*, 2020, **49**, 3222–3227.

74 I. Oyarzabal, J. Ruiz, E. Ruiz, D. Aravena, J. M. Seco and E. Colacio, Increasing the effective energy barrier promoted by the change of a counteranion in a Zn–Dy–Zn SMM: slow relaxation via the second excited state, *Chem. Commun.*, 2015, **51**, 12353–12356.

75 S. K. Singh, T. Gupta, M. Shanmugam and G. Rajaraman, Unprecedented magnetic relaxation via the fourth excited state in low-coordinate lanthanide single-ion magnets: a theoretical perspective, *Chem. Commun.*, 2014, **50**, 15513–15516.

76 M. Briganti, F. Santanni, L. Tesi, F. Totti, R. Sessoli and A. Lunghi, A Complete *Ab Initio* View of Orbach and Raman Spin–Lattice Relaxation in a Dysprosium Coordination Compound, *J. Am. Chem. Soc.*, 2021, **143**, 13633–13645.

77 Y.-S. Ding, K.-X. Yu, D. Reta, F. Ortu, R. E. P. Winpenny, Y.-Z. Zheng and N. F. Chilton, Field- and temperature-dependent quantum tunnelling of the magnetisation in a large barrier single-molecule magnet, *Nat. Commun.*, 2018, **9**, 3134.

78 D. Gatteschi, R. Sessoli and J. Villain, *Molecular Nanomagnets*, Oxford Academic, Oxford, 2006, pp. 58–61.

79 S. Alvarez, D. Avnir, M. Llunell and M. Pinsky, Continuous symmetry maps and shape classification. The case of six-coordinated metal compoundsESI (ESI) available: tables of CSD refcodes, structural parameters and symmetry measures for the studied compounds, *New J. Chem.*, 2002, **26**, 996–1009.

80 D. Gatteschi, R. Sessoli and J. Villain, *Molecular Nanomagnets*, Oxford Academic, Oxford, 2006, pp. 108–159.

81 R. Orbach, On the Theory of Spin-Lattice Relaxation in Paramagnetic Salts, *Proc. Phys. Soc.*, 1961, **77**, 821–826.

82 F. Neese, Software update: the ORCA program system, version 4.0, *Wiley Interdiscip. Rev.:Comput. Mol. Sci.*, 2018, **8**, e1327.

83 F. Neese, Software update: The ORCA program system—Version 5.0, *Wiley Interdiscip. Rev.:Comput. Mol. Sci.*, 2022, **12**, 1606.

84 F. Neese, F. Wennmohs, U. Becker and C. Riplinger, The ORCA quantum chemistry program package, *J. Chem. Phys.*, 2020, **152**, 224108.

85 F. Aquilante, J. Autschbach, R. K. Carlson, L. F. Chibotaru, M. G. Delcey, L. De Vico, I. F. Galván, N. Ferré, L. M. Frutos, L. Gagliardi, M. Garavelli, A. Giussani, C. E. Hoyer, G. Li Manni, H. Lischka, D. Ma, P. Å. Malmqvist, T. Müller, A. Nenov, M. Olivucci, T. B. Pedersen, D. Peng, F. Plasser, B. Pritchard, M. Reiher, I. Rivalta, I. Schapiro, J. Segarra-Martí, M. Stenrup, D. G. Truhlar, L. Ungur, A. Valentini, S. Vancoillie, V. Veryazov, V. P. Vysotskiy, O. Weingart, F. Zapata and R. Lindh, Molcas 8: New capabilities for multiconfigurational quantum chemical calculations across the periodic table, *J. Comput. Chem.*, 2015, **37**, 506–541.

86 L. F. Chibotaru and L. Ungur, Ab initio calculation of anisotropic magnetic properties of complexes. I. Unique definition of pseudospin Hamiltonians and their derivation, *J. Chem. Phys.*, 2012, **137**, 064112.

87 A. A. Granovsky, Extended multi-configuration quasi-degenerate perturbation theory: The new approach to multi-state multi-reference perturbation theory, *J. Chem. Phys.*, 2011, **134**, 214113.
88 D. Aravena, Ab Initio Prediction of Tunneling Relaxation Times and Effective Demagnetization Barriers in Kramers Lanthanide Single-Molecule Magnets, *J. Phys. Chem. Lett.*, 2018, **9**, 5327–5333.
89 Y. Gil and D. Aravena, Understanding Single-Molecule Magnet properties of lanthanide complexes from 4f orbital splitting, *Dalton Trans.*, 2024, **53**, 2207–2217.
90 W. J. A. Blackmore, G. K. Gransbury, P. Evans, J. G. C. Kragskow, D. P. Mills and N. F. Chilton, Characterisation of magnetic relaxation on extremely long timescales, *Phys. Chem. Chem. Phys.*, 2023, **25**, 16735–16744.
91 J. C. Vanjak, B. O. Wilkins, V. Vieru, N. S. Bhuvanesh, J. H. Reibenspies, C. D. Martin, L. F. Chibotaru and M. Nippe, A High-Performance Single-Molecule Magnet Utilizing Dianionic Aminoborolide Ligands, *J. Am. Chem. Soc.*, 2022, **144**, 17743–17747.
92 K. Randall McClain, C. A. Gould, K. Chakarawet, S. J. Teat, T. J. Groshens, J. R. Long and B. G. Harvey, High-temperature magnetic blocking and magneto-structural correlations in a series of dysprosium(III) metallocenium single-molecule magnets, *Chem. Sci.*, 2018, **9**, 8492–8503.
93 P. Evans, D. Reta, G. F. S. Whitehead, N. F. Chilton and D. P. Mills, Bis-Monophospholyl Dysprosium Cation Showing Magnetic Hysteresis at 48 K, *J. Am. Chem. Soc.*, 2019, **141**, 19935–19940.
94 K.-X. Yu, J. G. C. Kragskow, Y.-S. Ding, Y.-Q. Zhai, D. Reta, N. Chilton and Y.-Z. Zheng, Enhancing Magnetic Hysteresis in Single-Molecule Magnets by Ligand Functionalisation, *Chem*, 2020, **6**, 1777–1793.
95 L. R. Thomas-Hargreaves, M. J. Giansiracusa, M. Gregson, E. Zanda, F. O'Donnell, A. J. Wooles, N. F. Chilton and S. T. Liddle, Correlating axial and equatorial ligand field effects to the single-molecule magnet performances of a family of dysprosium bis-methanediide complexes, *Chem. Sci.*, 2021, **12**, 3911–3920.
96 P. Evans, D. Reta, C. A. P. Goodwin, F. Ortu, N. F. Chilton and D. P. Mills, A double-dysprosocenium single-molecule magnet bound together with neutral ligands, *Chem. Commun.*, 2020, **56**, 5677–5680.
97 S. Gupta, S. Dey, T. Rajeshkumar, G. Rajaraman and R. Murugavel, Deciphering the role of anions and secondary coordination sphere in tuning anisotropy in Dy(III) air-stable D_{5h} SIMs, *Chem. – Eur. J.*, 2022, **28**, e202103585.
98 S. Corner, G. Gransbury, I. Vitorica-Yrezabal, G. Whitehead, N. Chilton and D. Mills, Halobenzene adducts of a dysprosocenium single-molecule magnet, *Inorg. Chem.*, 2024, **63**, 9552–9561.
99 Y. Liu, Y.-C. Chen, J. Liu, W.-B. Chen, G.-Z. Huang, S.-G. Wu, J. Wang, J.-L. Liu and M.-L. Tong, Cyanometallate-Bridged Didysprosium Single-Molecule Magnets Constructed with Single-Ion Magnet Building Block, *Inorg. Chem.*, 2020, **59**, 687–694.
100 S. Demir, M. I. Gonzalez, L. E. Darago, W. J. Evans and J. R. Long, Giant coercivity and high magnetic blocking temperatures for N_2^{3-} radical-bridged dilanthanide complexes upon ligand dissociation, *Nat. Commun.*, 2017, **8**, 2144–2144.
101 W. Cai, J. D. Bocarsly, A. Gomez, R. J. Letona Lee, A. Metta-Magaña, R. Seshadri and L. Echegoyen, High blocking temperatures for DyScS endohedral fullerene single-molecule magnets, *Chem. Sci.*, 2020, **11**, 13129–13136.
102 S. Demir, J. M. Zadrozny, M. Nippe and J. R. Long, Exchange Coupling and Magnetic Blocking in Bipyrimidyl Radical-Bridged Dilanthanide Complexes, *J. Am. Chem. Soc.*, 2012, **134**, 18546–18549.
103 N. Mavragani, D. Errulat, D. A. Gálico, A. A. Kitos, A. Mansikkamäki and M. Murugesu, Radical–Bridged Ln_4 Metallocene Complexes with Strong Magnetic Coupling and a Large Coercive Field, *Angew. Chem., Int. Ed.*, 2021, **60**, 24206–24213.
104 M. J. Giansiracusa, S. Al-Badran, A. K. Kostopoulos, G. F. S. Whitehead, D. Collison, F. Tuna, R. E. P. Winpenny and N. F. Chilton, A large barrier single-molecule magnet without magnetic memory, *Dalton Trans.*, 2019, **48**, 10795–10798.
105 S. Bala, G.-Z. Huang, Z.-Y. Ruan, S.-G. Wu, Y. Liu, L.-F. Wang, J.-L. Liu and M.-L. Tong, A square antiprism dysprosium single-ion magnet with an energy barrier over 900 K, *Chem. Commun.*, 2019, **55**, 9939–9942.
106 M. Fondo, J. Corredoira-Vázquez, A. M. García-Deibe, J. Sanmartín-Matalobos, S. Gómez-Coca, E. Ruiz and E. Colacio, Slow magnetic relaxation in dinuclear dysprosium and holmium phenoxide bridged complexes: a Dy_2 single molecule magnet with a high energy barrier, *Inorg. Chem. Front.*, 2021, **8**, 2532–2541.
107 X.-Q. Ji, J. Xiong, R. Sun, F. Ma, H.-L. Sun, Y.-Q. Zhang and S. Gao, Enhancing the magnetic performance of pyrazine-*N*-oxide bridged dysprosium chains through controlled variation of ligand coordination modes, *Dalton Trans.*, 2021, **50**, 7048–7055.
108 H. Wu, M. Li, Z. Xia, V. Montigaud, O. Cador, B. Le Guennic, H. Ke, W. Wang, G. Xie, S. Chen and S. Gao, High temperature quantum tunnelling of magnetization and thousand kelvin anisotropy barrier in a Dy_2 single-molecule magnet, *Chem. Commun.*, 2021, **57**, 371–374.
109 Z. Zhu, C. Zhao, Q. Zhou, S. Liu, X.-L. Li, A. Mansikkamäki and J. Tang, Air-Stable Dy(III)-Macrocycle Enantiomers: From Chiral to Polar Space Group, *CCS Chem.*, 2022, **4**, 3762–3771.
110 X. L. Ding, Y. Q. Zhai, T. Han, W. P. Chen, Y. S. Ding and Y. Z. Zheng, A Local D_{4h} Symmetric Dysprosium(III) Single–Molecule Magnet with an Energy Barrier Exceeding 2000 K, *Chem. – Eur. J.*, 2021, **27**, 2623–2627.
111 J. Xiong, H.-Y. Ding, Y.-S. Meng, C. Gao, X.-J. Zhang, Z.-S. Meng, Y.-Q. Zhang, W. Shi, B.-W. Wang and S. Gao, Hydroxide-bridged five-coordinate Dy(III) single-molecule magnet exhibiting the record thermal relaxation barrier of

magnetization among lanthanide-only dimers, *Chem. Sci.*, 2017, **8**, 1288–1294.

112 P. B. Jin, Y. Q. Zhai, K. X. Yu, R. E. P. Winpenny and Y. Z. Zheng, Dysprosiacarboranes as Organometallic Single–Molecule Magnets, *Angew. Chem., Int. Ed.*, 2020, **59**, 9350–9354.

113 A. B. Canaj, S. Dey, O. Céspedes, C. Wilson, G. Rajaraman and M. Murrie, There is nothing wrong with being soft: using sulfur ligands to increase axiality in a Dy(iii) single-ion magnet, *Chem. Commun.*, 2020, **56**, 1533–1536.

114 K. L. M. Harriman, J. Murillo, E. A. Suturina, S. Fortier and M. Murugesu, Relaxation dynamics in see-saw shaped Dy(iii) single-molecule magnets, *Inorg. Chem. Front.*, 2020, **7**, 4805–4812.

115 S. Demir, M. D. Boshart, J. F. Corbey, D. H. Woen, M. I. Gonzalez, J. W. Ziller, K. R. Meihaus, J. R. Long and W. J. Evans, Slow Magnetic Relaxation in a Dysprosium Ammonia Metallocene Complex, *Inorg. Chem.*, 2017, **56**, 15049–15056.

116 Z.-H. Li, Y.-Q. Zhai, W.-P. Chen, Q.-C. Luo, T. Han and Y.-Z. Zheng, Breaking the axiality of pentagonal–bipyramidal dysprosium(III) single-molecule magnets with pyrazolate ligands, *Inorg. Chem. Front.*, 2020, **7**, 4367–4376.

117 M. Li, H. Wu, Z. Xia, L. Ungur, D. Liu, L. F. Chibotaru, H. Ke, S. Chen and S. Gao, An Inconspicuous Six-Coordinate Neutral DyIII Single-Ion Magnet with Remarkable Magnetic Anisotropy and Stability, *Inorg. Chem.*, 2020, **59**, 7158–7166.

118 J. Long, I. V. Basalov, N. V. Forosenko, K. A. Lyssenko, E. Mamontova, A. V. Cherkasov, M. Damjanović, L. F. Chibotaru, Y. Guari, J. Larionova and A. A. Trifonov, Dysprosium Single-Molecule Magnets with Bulky Schiff Base Ligands: Modification of the Slow Relaxation of the Magnetization by Substituent Change, *Chem. – Eur. J.*, 2018, **25**, 474–478.

119 H.-M. Dong, H.-Y. Li, Y.-Q. Zhang, E.-C. Yang and X.-J. Zhao, Magnetic Relaxation Dynamics of a Centrosymmetric Dy_2 Single-Molecule Magnet Triggered by Magnetic-Site Dilution and External Magnetic Field, *Inorg. Chem.*, 2017, **56**, 5611–5622.

120 T. Han, W. Shi, Z. Niu, B. Na and P. Cheng, Magnetic Blocking from Exchange Interactions: Slow Relaxation of the Magnetization and Hysteresis Loop Observed in a Dysprosium-Nitronyl Nitroxide Chain Compound with an Antiferromagnetic Ground State, *Chem. – Eur. J.*, 2012, **19**, 994–1001.

121 G. Lu, Y. Liu, W. Deng, G.-Z. Huang, Y.-C. Chen, J.-L. Liu, Z.-P. Ni, M. Giansiracusa, N. F. Chilton and M.-L. Tong, A perfect triangular dysprosium single-molecule magnet with virtually antiparallel Ising-like anisotropy, *Inorg. Chem. Front.*, 2020, **7**, 2941–2948.

122 S. Demir, M. Nippe, M. I. Gonzalez and J. R. Long, Exchange coupling and magnetic blocking in dilanthanide complexes bridged by the multi-electron redox-active ligand 2,3,5,6-tetra(2-pyridyl)pyrazine, *Chem. Sci.*, 2014, **5**, 4701–4711.

123 Z. H. Li, Y. Q. Zhai, W. P. Chen, Y. S. Ding and Y. Z. Zheng, Air–Stable Hexagonal Bipyramidal Dysprosium(III) Single–Ion Magnets with Nearly Perfect D_{6h} Local Symmetry, *Chem. – Eur. J.*, 2019, **25**, 16219–16224.

124 S. Jia, X. Zhu, B. Yin, Y. Dong, A. Sun and D.-f. Li, Macrocyclic Hexagonal Bipyramidal Dy(III)-Based Single-Molecule Magnets with a D6 h Symmetry, *Cryst. Growth Des.*, 2023, **23**, 6967–6973.

125 S.-S. Liu, Y.-S. Meng, Y.-Q. Zhang, Z.-S. Meng, K. Lang, Z.-L. Zhu, C.-F. Shang, B.-W. Wang and S. Gao, A Six-Coordinate Dysprosium Single-Ion Magnet with Trigonal-Prismatic Geometry, *Inorg. Chem.*, 2017, **56**, 7320–7323.

126 A. G. Bispo-Jr, L. Yeh, D. Errulat, D. A. Gálico, F. A. Sigoli and M. Murugesu, Improving the performance of β-diketonate-based DyIII single-molecule magnets displaying luminescence thermometry, *Chem. Commun.*, 2023, **59**, 8723–8726.

127 J.-W. Yang, Y.-M. Tian, J. Tao, P. Chen, H.-F. Li, Y.-Q. Zhang, P.-F. Yan and W.-B. Sun, Modulation of the Coordination Environment around the Magnetic Easy Axis Leads to Significant Magnetic Relaxations in a Series of 3d-4f Schiff Complexes, *Inorg. Chem.*, 2018, **57**, 8065–8077.

128 G. Velkos, D. S. Krylov, K. Kirkpatrick, L. Spree, V. Dubrovin, B. Büchner, S. M. Avdoshenko, V. Bezmelnitsyn, S. Davis, P. Faust, J. Duchamp, H. C. Dorn and A. A. Popov, High Blocking Temperature of Magnetization and Giant Coercivity in the Azafullerene $Tb_2@C_{79}N$ with a Single-Electron Terbium-Terbium Bond, *Angew. Chem., Int. Ed.*, 2019, **58**, 5891–5896.

129 J. D. Rinehart, M. Fang, W. J. Evans and J. R. Long, A N_2^{3-} Radical-Bridged Terbium Complex Exhibiting Magnetic Hysteresis at 14 K, *J. Am. Chem. Soc.*, 2011, **133**, 14236–14239.

130 Z. Hu, H. Hu, Z. Chen, D. Liu, Y. Zhang, J. Sun, Y. Liang, D. Yao and F. Liang, Guest-Induced Switching of a Molecule-Based Magnet in a 3d–4f Heterometallic Cluster-Based Chain Structure, *Inorg. Chem.*, 2020, **60**, 633–641.

131 K. R. Meihaus and J. R. Long, Magnetic Blocking at 10 K and a Dipolar-Mediated Avalanche in Salts of the Bis(η^8-cyclooctatetraenide) Complex $[Er(COT)_2]^-$, *J. Am. Chem. Soc.*, 2013, **135**, 17952–17957.

132 A. P. Orlova, J. D. Hilgar, M. G. Bernbeck, M. Gembicky and J. D. Rinehart, Intuitive Control of Low-Energy Magnetic Excitations via Directed Dipolar Interactions in a Series of Er(III)-Based Complexes, *J. Am. Chem. Soc.*, 2022, **144**, 11316–11325.

133 H. Kong, J.-Y. Wang, J.-C. Liu, L. Zhang, P.-Y. Liao, Y.-Q. Qi, Z. Liu, S.-G. Wu and M.-L. Tong, Photochromic Dysprosium Single-Molecule Magnet Featuring Reversible Redox Transformation of Polyoxomolybdate Moiety, *Angew. Chem., Int. Ed.*, 2024, e202422557.

134 S. K. Langley, D. P. Wielechowski, V. Vieru, N. F. Chilton, B. Moubaraki, B. F. Abrahams, L. F. Chibotaru and K. S. Murray, A $\{CrIII_2DyIII_2\}$ Single-Molecule Magnet:

Enhancing the Blocking Temperature through 3d Magnetic Exchange, *Angew. Chem., Int. Ed.*, 2013, **52**, 12014–12019.

135 B.-K. Ling, Y.-Q. Zhai, P.-B. Jin, H.-F. Ding, X.-F. Zhang, Y. Lv, Z. Fu, J. Deng, M. Schulze, W. Wernsdorfer and Y.-Z. Zheng, Suppression of zero-field quantum tunneling of magnetization by a fluorido bridge for a "very hard" 3d-4f single-molecule magnet, *Matter*, 2022, **5**, 3485–3498.

136 H. Kwon, K. R. McClain, J. G. C. Kragskow, J. K. Staab, M. Ozerov, K. R. Meihaus, B. G. Harvey, E. S. Choi, N. F. Chilton and J. R. Long, Coercive Fields Exceeding 30 T in the Mixed-Valence Single-Molecule Magnet $(CpiPr_5)_2Ho_2I_3$, *J. Am. Chem. Soc.*, 2024, **146**, 18714–18721.

137 J. M. Zadrozny, D. J. Xiao, M. Atanasov, G. J. Long, F. Grandjean, F. Neese and J. R. Long, Magnetic blocking in a linear iron(I) complex, *Nat. Chem.*, 2013, **5**, 577–581.

138 A. W. Cook, J. D. Bocarsly, R. A. Lewis, A. J. Touchton, S. Morochnik and T. W. Hayton, An iron ketimide single-molecule magnet $[Fe_4(N{=}CPh_2)_6]$ with suppressed through-barrier relaxation, *Chem. Sci.*, 2020, **11**, 4753–4757.

139 M. Heu, S. Yoon, B. J. Suh, D.-Y. Jung, J. W. Suk and Y. J. Kim, Magnetic Relaxation in a Single-Molecule Magnet Mn_{12}-chlorobutylate, *J. Korean Phys. Soc.*, 2003, **43**, 544–547.

140 S. Verma, A. Verma, A. K. Srivastava, A. Gupta, S. P. Singh and P. Singh, Structural and magnetic properties of Mn_{12}-Stearate nanomagnets, *Mater. Chem. Phys.*, 2016, **177**, 140–146.

141 M. Laskowska, O. Pastukh, P. Konieczny, M. Dulski, M. Zalsiński and L. Laskowski, Magnetic Behaviour of Mn_{12}-Stearate Single-Molecule Magnets Immobilized on the Surface of 300 nm Spherical Silica Nanoparticles, *Materials*, 2020, **13**, 2624.

142 A. Verma, S. Verma, P. Singh and A. Gupta, Ageing effects on the magnetic properties of Mn_{12}-based Acetate and Stearate SMMs, *J. Magn. Magn. Mater.*, 2017, **439**, 76–81.

143 L. A. Kushch, V. D. Sasnovskaya, A. I. Dmitriev, E. B. Yagubskii, O. V. Koplak, L. V. Zorina and D. W. Boukhvalov, New single-molecule magnet based on Mn_{12} oxocarboxylate clusters with mixed carboxylate ligands, $[Mn_{12}O_{12}(CN\text{-}o\text{-}C_6H_4CO_2)_{12}(CH_3CO_2)_4(H_2O)_4]\cdot 8CH_2Cl_2$: Synthesis, crystal and electronic structure, magnetic properties, *Dalton Trans.*, 2012, **41**, 13747–13754.

144 D. Wu, D. Guo, Y. Song, W. Huang, C. Duan, Q. Meng and O. Sato, CoII Molecular Square with Single-Molecule Magnet Properties, *Inorg. Chem.*, 2009, **48**, 854–860.

145 S. K. Gupta, H. H. Nielsen, A. M. Thiel, E. A. Klahn, E. Feng, H. B. Cao, T. C. Hansen, E. Lelièvre-Berna, A. Gukasov, I. Kibalin, S. Dechert, S. Demeshko, J. Overgaard and F. Meyer, Multi-Technique Experimental Benchmarking of the Local Magnetic Anisotropy of a Cobalt(II) Single-Ion Magnet, *JACS Au*, 2023, **3**, 429–440.

146 K. Qian, X.-C. Huang, C. Zhou, X.-Z. You, X.-Y. Wang and K. R. Dunbar, A Single-Molecule Magnet Based on Heptacyanomolybdate with the Highest Energy Barrier for a Cyanide Compound, *J. Am. Chem. Soc.*, 2013, **135**, 13302–13305.